Estimating saturation and density changes caused by CO_2 injection at Sleipner — Using time-lapse seismic amplitude-variation-with-offset and time-lapse gravity

Martin Landrø[1] and Mark Zumberge[2]

Abstract

We have developed a calibrated, simple time-lapse seismic method for estimating saturation changes from the CO_2-storage project at Sleipner offshore Norway. This seismic method works well to map changes when CO_2 is migrating laterally away from the injection point. However, it is challenging to detect changes occurring below CO_2 layers that have already been charged by some CO_2. Not only is this partly caused by the seismic shadow effects, but also by the fact that the velocity sensitivity for CO_2 change in saturation from 0.3 to 1.0 is significantly less than saturation changes from zero to 0.3. To circumvent the seismic shadow zone problem, we combine the time-lapse seismic method with time-lapse gravity measurements. This is done by a simple forward modeling of gravity changes based on the seismically derived saturation changes, letting these saturation changes be scaled by an arbitrary constant and then by minimizing the least-squares error to obtain the best fit between the scaled saturation changes and the measured time-lapse gravity data. In this way, we are able to exploit the complementary properties of time-lapse seismic and gravity data.

Introduction

To estimate rock density directly from seismic data is challenging and associated with high uncertainties. Prestack inversion methods exploiting amplitude-variation-with-offset (AVO) information have been tested to estimate P-wave velocity, S-wave velocity, and density simultaneously by several researchers. Helgesen and Landrø (1993) formulate an AVO-inversion scheme in which P- and S-wave velocities, densities, and layer thicknesses were inverted for. Buland et al. (1996) use a nonlinear AVO-inversion in the τ-ρ domain to estimate these three parameters at the Troll Field, offshore Norway. Leiceaga et al. (2010) use multicomponent data to reduce the uncertainty related to inversion of density. Bai and Yingst (2014) test full-waveform inversion (FWI) on synthetic data and find that it is challenging to avoid crosstalk between velocity and density. Roy et al. (2006) explore the possibility of using wide-angle data for density inversion and find that by incorporating incidence angles from 40° to 55°, more stable and reliable density estimates can be achieved. However, such data must be processed with care, and it often involves anisotropic imaging and wavelet stretch corrections. Despite the fact that there have been significant research efforts on how to estimate density reliably from seismic data, it is still considered to be difficult (Roy et al., 2008) and much more unstable compared with impedance inversion.

For time-lapse seismic data, we find more or less the same challenges; however, the possibility of extracting density information might be somewhat better in cases in which high-quality repeated surveys are undertaken. For time-lapse seismic data, when oil or gas is replaced with water, for example, there is a linear relationship between the saturation and density changes. Therefore, for 4D seismic data, one can say that density estimation is to some extent equivalent to estimating saturation changes. There are several examples of saturation estimation from time-lapse seismic data (see for example, Landrø, 1999, 2001; Tura and Lumley, 1999; Trani et al., 2011; Grude et al., 2013; Bhakta and Landrø, 2014). If the saturation is not uniform (patchy), then the rock-physics relations between saturation and seismic parameters should be changed (Grude et al., 2013).

Our goal is to combine saturation estimates from time-lapse seismic data with repeated gravity measurements to reduce the large uncertainty related to time-lapse estimated density changes. For this purpose, we use data acquired at the Sleipner CO_2 storage site. Since Statoil launched this project in 1996, more than 150 papers have been published on various topics attached to this project. Several seismic surveys and complementary data have

[1]Norwegian University of Science and Technology, Department of Geoscience and Petroleum, Trondheim, Norway. E-mail: martin.landro@ntnu.no.

[2]University of California, Scripps Institution of Oceanography, San Diego, California, USA. E-mail: mzumberge@ucsd.edu.

Manuscript received by the Editor 7 July 2016; revised manuscript received 30 October 2016; published online 05 April 2017. This paper appears in *Interpretation*, Vol. 5, No. 2 (May 2017); p. T243–T257, 21 FIGS., 2 TABLES.

http://dx.doi.org/10.1190/INT-2016-0120.1.

been made available to researchers, and therefore, it is expected that a variety of analyses will continue to grow in the future. Arts et al. (2008) publish an overview of the seismic results achieved after 10 years of CO_2 injection, in which they discuss combined use of time-lapse seismic and gravity. One major difference between our paper and Arts et al. (2008) is that we derive explicit expressions for saturation changes using time-lapse seismic AVO-data as an input. Furthermore, we limit these estimates by using gravity measurements in the inversion procedure. Queißer and Singh (2013) use a 2D FWI scheme to invert for P-wave velocity using prestack time-lapse seismic data from 1994 and 1999. Rabben and Ursin (2011) use the 2001 seismic data and perform an amplitude-variation-with-angle inversion for the top Utsira Formation and estimate P- and S-wave impedances as well as density. They clearly show the potential for using amplitude information to distinguish between acoustic impedance and density at Sleipner. Evensen and Landrø (2010) use a time-lapse tomographic inversion method and seismic data sets from 1994 and 2001 to estimate the P-wave velocity in a thin CO_2 layer.

In 1996, Statoil and the Scripps Institution of Oceanography embarked on a project to develop high-precision seafloor gravimeters focusing on accurate measurements of density changes caused by hydrocarbon production in a reservoir or storage of CO_2 in the subsurface (Sasagawa et al., 2003; Zumberge et al., 2008). Here, we combine the gravimetric results published in Alnes et al. (2011) with seismic estimation of saturation changes between 2001 and 2008.

Another way to constrain and help the interpretation of 4D seismic data acquired above the CO_2-storage sites is to use fluid flow simulation techniques. Some of the early published simulation results were published by Lindeberg and Bergmo (2003), and a more recent example can be found in Cavanagh and Hazeldine (2014).

This paper is organized as follows: First, we present the input data: time-lapse seismic and gravity data. An overview of the basic assumptions made in the paper is given in the next section. A simple rock-physics model based on earlier work is presented as a basis for this analysis. Then, we derive a simple formula relating near- and far-offset time-lapse changes directly to saturation changes, based on the rock-physics model. The calibration procedure used to couple seismic amplitude changes directly to saturation changes is described in a separate section. A key section in the paper is the formulation of a simple inversion problem to combine measured time-lapse seismic data with the measured gravity anomalies. Before we conclude, we discuss various limitations and precautions for the presented work.

The input data

The input seismic data used in this project are listed in Table 1. Note that what we refer to here as the far-offset stack (450–1050 m) is not the stack containing the largest offsets. Offsets from 1200 to 1650 m were collected, but these are not used due to significantly lower 4D repeatability of this stack. In this project, our aim is to study 4D changes in AVO, and, hence, we need to use data that are highly repeatable. The average incidence angle using simple ray tracing for the near-offset stack (150–450 m) is approximately 11°, and the corresponding angle for our far-offset data (600–1050 m) is approximately 30°. A moderate Q-filter assuming a constant Q-value of 300 was used in the processing of the seismic data. The remaining amplitude compensation was done consistently for the 2001 and 2008 seismic data sets. Therefore, we will assume that apart from an additional Q-compensation that we introduce, there should be only one global scalar necessary to convert the seismic data into "true" reflectivity. Because we use a root-mean-square (rms) window technique to extract reflection amplitudes, this scalar will vary with the length of the window we are using, and hence the global scalar will increase as the length of the rms window increases.

The injection of CO_2 at Sleipner started in 1999. This means that the 2001 data set that we are using as a baseline is not a true baseline survey because some changes had already occurred when the 2001 survey was acquired. Hence, we have to roughly estimate the extent and saturation in 2001 based on the 2001 data only, and this is done by assuming that the amplitude anomaly observed close to the injection well on the 2001 seismic data is mainly caused by the CO_2 injection. A better choice would of course be to use data from 1994 (which unfortunately were not available to us during this project) and to use the time-lapse seismic difference between 2001 and 1994 to estimate the saturation distribution in 2001.

Time-lapse gravity data from 2002 and 2009 are also used, and here, we have used the same data as those presented by Alnes et al. (2011). The seismic data and the gravity data cover approximately the same number of years (seven); how-

Table 1. An overview of available offset stacks. Those that were actually used in this study are marked by green. Note that what we refer to as far offset here (corresponding to an average reflection angle of approximately 30°) does not represent the offset stack including the largest offsets.

Data type	150–450 m offset stack NEAR	600–1050 m offset stack FAR	1200–1650 m offset stack ULTRA FAR
2001 3D seismic	Used	Used	Not used
2008 3D seismic	Used	Used	Not used

ever, the gravity data have a delay of one year compared with the seismic data. We will assume that this delay is zero and that the seismic and gravity time-lapse data were acquired simultaneously. It is hard to assess or quantify the error caused by this assumption.

Some basic assumptions

Because this is a combined methodology and case study, we have to make several assumptions. Some of these assumptions are based on scientific considerations, and others are used to simplify the case study. Below we give a list of such assumptions and add some comments to each item:

- We assume that the empirical relations given by Span and Wagner for CO_2 at various pressures and temperatures are valid. The initial reservoir temperature at the injection point is measured to be 35.5°C (Alnes et al., 2011). The initial pore pressure is hydrostatic, which means that it is 80 bar at 800 m depth, and hence, it is reasonable to assume that the injected CO_2 is most likely supercritical because the critical point is at 31°C and 74 bar.
- We assume that when supercritical CO_2 is injected into the brine-filled sandstone rock, the two liquids are immiscible and that the CO_2 pushes the water away from the injection point.
- A calibration procedure is needed to convert seismic amplitudes into reflection coefficients that are used for the AVO inversion. Our choice is to use one global scalar for this purpose. Ghaderi and Landrø (2007) find a near-offset reflection coefficient of −0.06 for the top sand layer outside the plume. This value was used to determine this global scalar (again using seismic data outside the CO_2 plume) to 0.02.
- We use a simple constant Q-model to account for amplitude variations between near- and far-offset stacks. (We found that $Q = 80$ was a good choice.) This is explained in Appendix A.
- Because we are using seismic data from 2001 and 2008, we need an estimate for the saturation change from 1996 (injection start) to 2001. We have assumed that the average CO_2 saturation was 0.1 in 2001. Here, 3 Mtons of CO_2 has been injected into the reservoir in the period between 1996 and 2001.
- We assume that the AVO response of many thin CO_2 layers can be approximated by using one thick layer and Backus averaging. This is a rough approximation, and we regard this as the lowest order approximation to the time-lapse seismic AVO-tuning problem. This issue is discussed in more detail in Appendix B.
- We assume that the average reservoir thickness or the thickness of the Utsira sand layer is approximately 200 m. From the seismic data, we estimate that the top reservoir varies by approximately 15 m and that the base has somewhat larger variations over the areas where the CO_2 plume occurs.
- We assume that saturation effects dominate over temperature and pore pressure on the time-lapse seismic data. This is mainly motivated by the dramatic decrease in P-wave velocity caused by a relatively small change in CO_2 saturation, and the fact that the pressure and temperature changes are moderate in the Sleipner CO_2 project.

A simple rock-physics model for CO_2 injection at Sleipner

We will assume that the CO_2 that is injected into the Utsira sand layer at Sleipner is supercritical and does not mix with the brine water that occupies the pore space prior to injection. In a P-T phase diagram, the typical pore pressure in the Utsira Formation is greater than 80 bar, and the temperature is most likely greater than 30°C, which leads to a supercritical state of CO_2. This is discussed by Alnes et al. (2011) who mention that the injected CO_2 at Sleipner is close to the critical point. Furthermore, we assume that the porosity is constant and equal to 37%. Ghaderi and Landrø (2009) use the empirical relations obtained by Span and Wagner (1996) to estimate the bulk modulus and density of the injected CO_2. It is important to notice that the density is strongly dependent on temperature and pressure at the storage site. For example, a temperature increase from 30 to 40°C reduces the CO_2 density from 680 to 300 kg/m^3, assuming that the pore pressure is 80 bar. Therefore, Ghaderi and Landrø (2009) present two curves (Figure 4 in their paper) representing the P-wave velocity change as a function of CO_2 saturation. In this paper, we use a simple exponential decay curve to model how the P-wave velocity α change with CO_2 saturation S within the Utsira sand (using a porosity value of 37%):

$$\alpha = \alpha_1 + \alpha_2 e^{-\kappa S}. \tag{1}$$

Here, $\alpha_1 = 1437$ m/s, $\alpha_2 = 613$ m/s, and $\kappa = 10$ was found by simple trial-and-error curve fitting and compared with Figure 4 in Ghaderi and Landrø (2009). This empirical formula represents an average between the two curves used in Ghaderi and Landrø (2009). The important feature of equation 1 is that it captures the steep decrease in velocity when the CO_2 saturation increases from zero to 0.1, as shown in Figure 1. Assuming nonmiscible mixture of CO_2 and water in the pore space, the fluid density ρ_F is a linear combination of the two phases:

$$\rho_F = S\rho_{CO_2} + (1 - S)\rho_W, \tag{2}$$

where W denotes water, which we assume has a density equal to 1050 kg/m^3. Alnes et al. (2011) discuss the ranges for densities within the Utsira Formation. The initial reservoir temperature is 35.5°C at the injection point at 1050 m. (The corresponding fluid pressure is then 105 bar.) Alnes et al. (2011) estimate the well-bottom CO_2 temperature to be 48°C, and using a fluid pressure

of 105 bar, they find a density of 485 kg/m^3. At the top Utsira, the corresponding density value is as low as 425 kg/m^3. However, they conclude that the average CO_2 density within the Utsira Formation is 675 kg/m^3. Therefore, we will use this value in most of our calculation and we use the 425 values as an extreme low-density value.

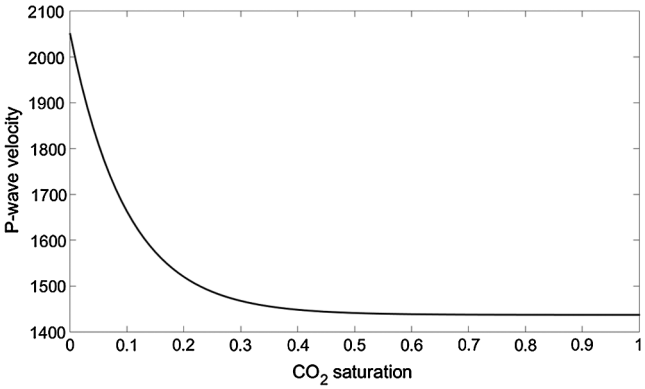

Figure 1. P-wave velocity versus CO_2 saturation using equation 1.

Table 2. Relative changes in P-wave velocity and density for the four time-lapse scenarios.

Change in CO_2 saturation	Relative P-wave velocity change	Relative density change assuming $\rho_{CO_2} = 675$ kg/m^3	Relative density change assuming $\rho_{CO_2} = 425$ kg/m^3
0 to 0.2	−0.24	−0.014	−0.023
0 to 0.5	−0.28	−0.034	−0.056
0.2 to 0.5	−0.06	−0.021	−0.034
0.5 to 1.0	−0.02	−0.035	−0.060

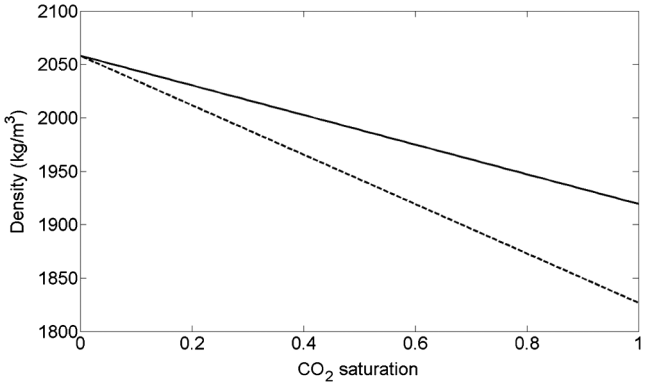

Figure 2. Rock density versus CO_2 saturation assuming that the density of CO_2 is 675 (solid line) and 425 kg/m^3 (dashed line).

The density of the rock including the fluid in the pore space is given as

$$\rho = \varphi\rho_F + (1-\varphi)\rho_S, \tag{3}$$

where $\varphi = 0.37$ is porosity and $\rho_S = 2650$ kg/m^3 is the density of the rock matrix or, in this case, the density of the quartz minerals. The density versus CO_2 saturation is shown in Figure 2 for the two end members of 675 and 435 kg/m^3 of CO_2 density. The expected relative changes in P-wave velocity and density are summarized in Figure 3. We notice that the relative velocity changes are large for saturation changes between zero and 0.4. The relative density changes are small (less than 0.05) in most cases, and hence, it is more appropriate to estimate velocity changes for the Sleipner CO_2 case. We will, therefore, estimate density changes caused by CO_2 injection by first estimating the saturation changes and then by estimating the density change by combining equations 2 and 3:

$$\Delta\rho = \varphi\Delta S(\rho_{CO_2} - \rho_W). \tag{4}$$

Assuming that the density difference between CO_2 and water is not varying spatially, we see that the density change is directly proportional to the saturation change. However, it is very likely (see the "Discussion" section in Alnes et al., 2011) that the density of CO_2 decreases away from the injection point because the injected CO_2 is gradually cooled by the surrounding rock as it propagates away from the injection point. For simplicity, we will assume that this effect is second order and we assume that the observed density changes from time-lapse gravity can be directly compared with the estimated saturation changes from the time-lapse seismic data.

A simple method to estimate density changes

It is inherently difficult to estimate density directly from seismic data. In seismic inversion, it is commonly accepted that it is robust and stable to estimate seismic impedance. The same is the case for time-lapse seismic data: There are few examples in which density changes have been estimated, and in most cases, this means to estimate saturation changes, and then derive density directly from the estimated saturation changes. Landrø (2001) formulates a direct-inversion method using time-lapse AVO data to estimate pressure and saturation changes in a producing hydrocarbon reservoir, or alternatively in an injection site of CO_2. Using equation 7 in Landrø (2001), we find that the change in P-wave reflection coefficient ΔR, when the pore fluid saturation changes, is given as

$$\Delta R = \frac{1}{2}\left(\frac{\Delta\rho}{\rho} + \frac{\Delta\alpha}{\alpha}\right) + \frac{\Delta\alpha}{2\alpha}\tan^2\theta, \quad (5)$$

where θ is the incidence angle, α is the P-wave velocity, ρ is the density, and Δ represents the time-lapse changes in the parameters. We will use this to directly invert for density changes. In the following sections, we will assume that the top reservoir has a clear amplitude increase when shale is overlaying CO_2-filled sandstone rock compared with when the same rock is filled with water. Next, we will assume that the time-lapse Δ in equation 5 represents the difference between water-filled and CO_2-filled rocks. This means that it is straightforward to estimate changes in the near- and far-offset stacks (ΔN and ΔF) between the two regions. We will further assume that these stacks have been calibrated to modeled reflection coefficients (as described in the "Calibrating time-lapse AVO data" section) so that they represent reflection coefficients. The time-lapse amplitude changes at near and far offsets are given (where θ_N and θ_F are the near- and far-offset angles) as

$$\Delta N = \frac{1}{2}\left(\frac{\Delta\rho}{\rho} + \frac{\Delta\alpha}{\alpha}\right) + \frac{\Delta\alpha}{2\alpha}\tan^2\theta_N \quad (6)$$

and

$$\Delta F = \frac{1}{2}\left(\frac{\Delta\rho}{\rho} + \frac{\Delta\alpha}{\alpha}\right) + \frac{\Delta\alpha}{2\alpha}\tan^2\theta_F. \quad (7)$$

Subtracting equations 7 and 6, we find an explicit expression for the change in P-wave velocity:

$$\frac{\Delta\alpha}{\alpha} = \frac{2(\Delta F - \Delta N)}{\tan^2\theta_F - \tan^2\theta_N}. \quad (8)$$

Substituting this back again into equation 6, we find an expression for the relative density change:

$$\frac{\Delta\rho}{\rho} = 2\Delta N - 2\frac{(\Delta F - \Delta N)}{\tan^2\theta_F - \tan^2\theta_N} \times (1 + \tan^2\theta_N). \quad (9)$$

The nice feature of this equation is that it is simple and represents a direct seismic estimate of the density contrast between water-filled and CO_2-filled reservoir rocks. However, one obvious problem is that the assumption behind equations 8 and 9 is that all relative contrasts should be much less than one. In many cases, these assumptions hold true, and in such cases, these equations are valid. It is also possible to include higher order terms. However, for our CO_2-injection case at Sleipner, the above equations are not sufficiently accurate. The relative P-wave velocity change is expected to be larger than 20% for the Sleipner CO_2 example. Therefore, we will use a slightly different version of equation 5 in which we assume that because the P-wave velocity effect is the dominant effect, an acoustic approximation will be sufficient. Assuming that we can use an acoustic approximation for the Zoeppritz equation, we get

$$\Delta R = \frac{1}{2}\left(\frac{\Delta\rho}{\rho} + \frac{\Delta\alpha}{\alpha}\right) + \frac{\Delta\alpha}{2\alpha}\sin^2\theta. \quad (10)$$

Because equations 5 and 10 only differ in the angle-dependent term, we replace tangent by sine in equations 8 and 9 to obtain the alternative and more accurate equations for the Sleipner CO_2 case. A comparison be-

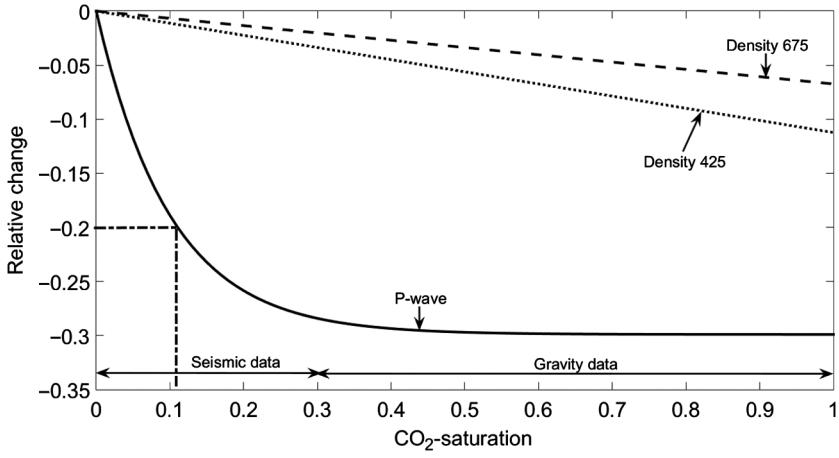

Figure 3. Relative change (change divided by original value) in P-wave velocity (solid line) and density assuming CO_2 density is of 675 kg/m^3 (dashed line) and density assuming CO_2 density of 425 kg/m^3 (dotted line) versus CO_2 saturation. A relative velocity change of −0.2 corresponds to a saturation change of 0.11, as shown by the dashed-dotted line. The two double arrows indicate which saturation bands we use for time-lapse seismic and gravity data, respectively, in this paper.

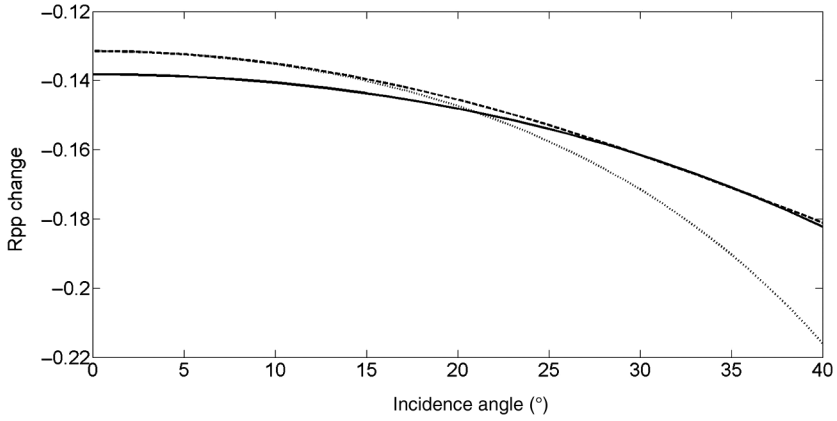

Figure 4. Modeling reflectivity changes using Zoeppritz equation (solid line), equation 5 (dotted line), and equation 10 (dashed line). Input parameters are listed in first column of Table 2.

tween equations 5 and 10 with the exact Zoeppritz equation is shown in Figure 4, using realistic values from the Sleipner CO_2 case. We see that equation 10 is more accurate in predicting the AVO behavior for the far offsets. Both approximations show a minor discrepancy of approximately 6%–7% at zero offset, which is caused by the simplification of replacing the zero-offset reflection coefficient by the first term on the right side in equation 10 (or 5).

Estimating CO_2-saturation changes

If we assume that the CO_2 saturation of the time for the first seismic survey A is S_A and the corresponding saturation for the second survey B is S_B, we find from equation 1 that the change in P-wave velocity is

$$\Delta\alpha = \alpha_1 + \alpha_2 e^{-\kappa S_B} - (\alpha_1 + \alpha_2 e^{-\kappa S_A}), \tag{11}$$

and hence the relative velocity change is given by

$$\frac{\Delta\alpha}{\alpha} = \frac{\alpha_2(e^{-\kappa S_B} - e^{-\kappa S_A})}{\alpha_1 + \alpha_2 e^{-\kappa S_A}}. \tag{12}$$

Combining this with equation 8, we find that the CO_2 saturation at time B is given as

$$S_B = -\frac{1}{\kappa}\ln\left[e^{-\kappa S_A} + 2\frac{(\Delta F - \Delta N)(\alpha_1 + \alpha_2 e^{-\kappa S_A})}{\alpha_2(\sin^2\theta_F - \sin^2\theta_N)}\right]. \tag{13}$$

The difference between the near- and far-offset seismic stacks is measured, and the angle span is known; hence, the most critical issue is to determine the CO_2 saturation for the first survey. Estimating CO_2 saturation from time-lapse seismic data becomes unstable for saturation values greater than 0.3–0.4 because there are practically no velocity changes when the saturation is increased from 0.3 to one (Figure 3). Therefore, this equation must be used with great care, and it definitely must be limited to saturation values of less than 0.3. Furthermore, we observe that the saturation change is directly dependent on the difference between the time-lapse far- and near-offset differences. This means that it is critical to calibrate the near- and far-offset differences prior to using equation 13. For example, if the argument to the logarithmic function in equation 13 is negative, it means that the calibration of the near- and far-offset reflectivity changes is poor. In practice, to avoid problems related to negative arguments for the logarithm in equation 13, we set S_B equal to 0.4 if this occurs. The value of 0.4 is chosen based on trial and error and is also related to the point in which the P-wave variation with CO_2 saturation flattens. Furthermore, we observe from Figure 4 that there is a minor discrepancy between Zoeppritz modeling and equation 10 (which is used to derive equation 13) for near offsets. This discrepancy can be reduced by introducing higher order terms in equation 10 (which then will lead to a corresponding modification of equation 13).

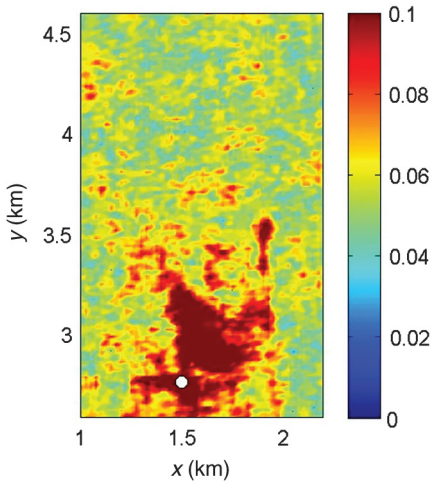

Figure 5. The rms amplitudes for near-offset stack from 2001 using a 26 ms time window. The injection point is shown as a white circle, and the dark red anomaly extending to the north and south to the injection point is caused by the CO_2 plume. In the north of approximately 3.5 km, we assume that there is no CO_2 in 2001, and we will therefore assume that the reflectivity above this line should represent the untouched reservoir. The color scale (0–0.1) represents absolute values of the reflection coefficient for the top Utsira interface.

Calibrating time-lapse AVO data

In equation 13, it is assumed that near- and far-offset seismic data have been calibrated so that they represent true reflectivity changes. In our calibration procedure, we will first scale the near-offset and far-offset seismic data by one constant scalar. From rock-physics modeling and well information, Ghaderi and Landrø (2009) find a near-offset reflection coefficient of −0.06 in a water-filled part of the top sand layer (outside the CO_2 plume). We find that by applying a global scalar of 0.02, the estimated rms amplitudes using a 26 ms time window gives a zero-offset reflection strength of approximately 0.06 for the untouched part of the reservoir, as shown in Figure 5.

Near- and far-offset stacks of the data for two crosslines are shown in Figures 6 and 7, in which the first crossline intersects the CO_2-injection point. We notice that the CO_2 effect on the seismic data is significant, on near- and far-offset data. This is consistent with the rock-physics model and corresponds well with the modeled velocity and density changes displayed in Figures 1–3. The top of the upper sand layer has a depth variation of the order of 15 ms within the plume mapped in 2008 (Figure 8). In our analysis, this depth variation has been included in a very simple way by adding a stepwise start time for the 26 ms time window used from the north to south, so that the added time for the southern areas is approximately 15 ms. In this way, we ensure that the rms signal captures the main seismic reflection associated with the top sand layer. We also tried to use the minimum and maximum values within the time window, and we found similar spatial maps when using the rms window, and, therefore, we decided to use rms as a way to

estimate reflection coefficients from the near- and far-offset data.

The next step is to find the relative scaling between the near- and far-offset stacks; we use a constant Q-model (see Appendix A) for the overburden to correct for the extra geometric damping of the far-offset data. Prior to this calibration step, we modeled four different scenarios based on the simple rock-physics model discussed above. The four scenarios are given in Table 2, which include CO_2-saturation changes from 0 to 0.2, 0 to 0.5, 0.2 to 0.5, and finally 0.5 to 1.0. The reflection coefficients versus angle for the four cases are shown in Figure 9. We notice that for the two latter scenarios, the overall differences and the AVO-differences are small, as expected. The seismic data are not very sensitive to saturation changes greater than 0.4. On the contrary, the two first scenarios show significant reflectivity differences at zero offset as well as a slight AVO increase with offset. In 2001, the extent of the plume for the uppermost CO_2 layer was limited to the area close to the injection point. In 2008, the extent of the seismic anomaly caused by CO_2 injection has increased significantly (Figure 10) and has followed the structurally higher areas toward the north. We find that the largest changes in reflectivity (for near- and far-offset data) occur approximately 1.4 km northeast of the injection point. At this point (or area), we observe an rms-difference change of approximately −0.14 (Figure 10). This near-offset value (shown by a black star in Figure 9) corresponds very well with the modeled black solid line in Figure 9. This means that the global scalar of 0.02 is consistent with the observed rms near-offset differences, given that the saturation has changed from zero to 0.2 in this area. The next step is to calibrate the far-offset difference data. From the modeled curve, we observe that the far-offset rms amplitude difference should be somewhat larger in magnitude and close to −0.16. By using a constant Q-model and assuming a Q-value of 80, we obtain an rms-difference value that is in perfect agreement with the modeled curve in Figure 9. From Figure 10, we see the effect of applying this Q-compensation to the far-offset data: The Q-compensated far-offset difference data (Figure 10c) is somewhat stronger in amplitude compared with the uncompensated data (Figure 10b). In summary, we have now used one global scalar (equal to 0.02) to convert the data from seismic amplitude values into reflection coefficient values, and another calibration step to calibrate the far-offset data by using a constant Q-model. For the calibration area (1.4 km northeast of the injection well), the observed near- and far-offset amplitude changes correspond to a saturation change from zero to 0.2.

It should be noted that if we assume that the saturation change is 0.5 instead of 0.2, a similar correction (us-

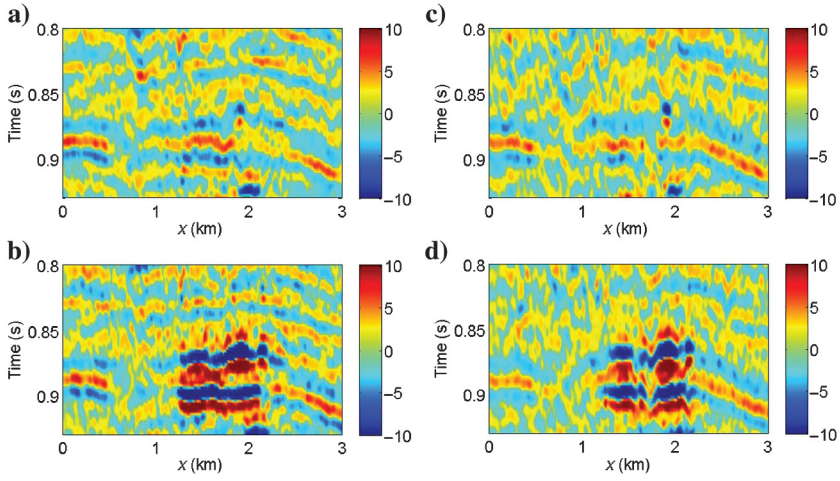

Figure 6. (a and b) Near-offset stacks from (a and c) 2001 and (b and d) 2008, and (c and d) corresponding far-offset stacks for crossline 1120. This crossline intersects the injection point at approximately 1.5 km. The color bar represents the original seismic amplitudes after processed into near- and far-offset stacks. The location of crossline 1120 is shown in Figure 10, and the direction is from the west to east.

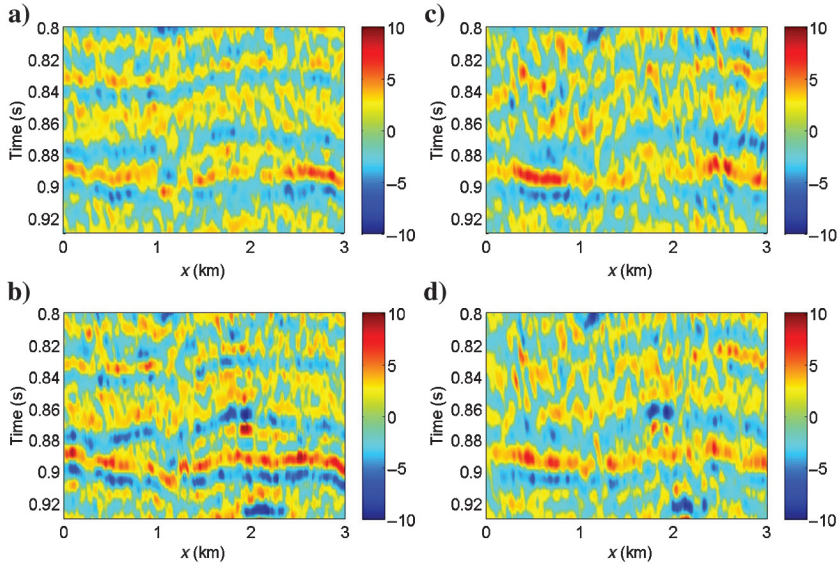

Figure 7. (a and b) Near-offset stacks from (a and c) 2001 and (b and d) 2008, and (c and d) corresponding far-offset stacks for crossline 1258. This is approximately 1 km north of the injection point. The CO_2 anomaly is observed for the 2008 at $x = 1.9$ km. The color bar represents the original seismic amplitudes after processed into near- and far-offset stacks. The location of crossline 1258 is shown in Figure 10, and the direction is from the west to east.

ing $Q = 80$) would still give a reasonable fit to this curve (shown by the red solid line in Figure 9). This is because the two curves for the two first scenarios are close to parallel. The estimated near-offset time-lapse difference after application of the 0.02 correction is shown in Figure 10 together with uncorrected and Q-compensated far-offset time-lapse difference. A time window of 26 ms has been used to estimate rms amplitudes prior to the calibration steps. After these two calibration steps, we are ready to use equation 13 to estimate saturation changes between 2001 and 2008. It should be noted that if the analysis is extended by using longer time windows for the rms calculation, the scaling factor (which is 0.02 for a 26 ms long window) should also be changed accordingly.

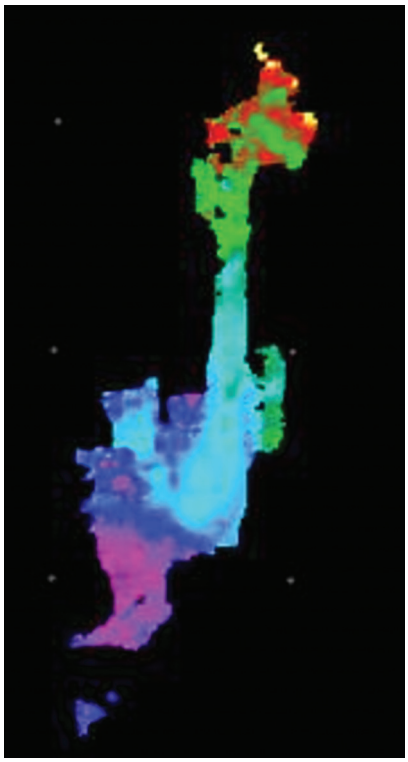

Figure 8. Top of Utsira time surface. Deep purple colors in the south correspond to 872 ms and red colors in the north correspond to 857 ms. Figure provided by Statoil. The size of the figure is approximately 1.8 km (horizontal) × 5 km (vertical).

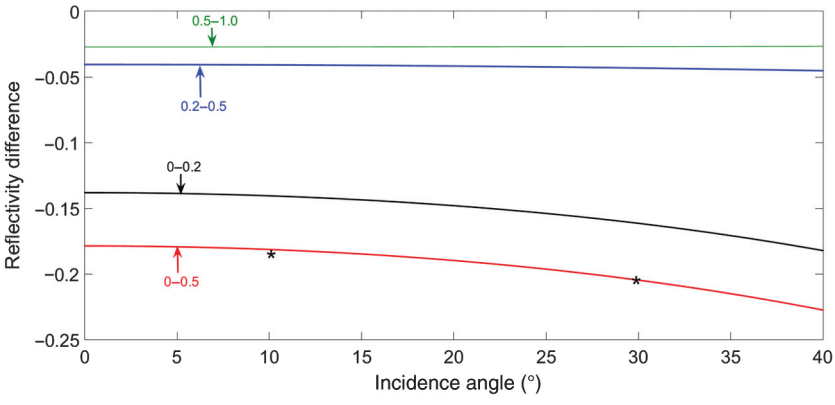

Figure 9. Zoeppritz AVO curves for four CO_2-saturation change scenarios: 0–0.2 (black line), 0–0.5 (red line), 0.2–0.5 (blue line), and 0.5–1.0 (green line). Calibration of far-offset stack data was obtained by using the black curve: First, the near- and far-offset data were multiplied with 0.02 based on the near-offset reflectivity outside the plume. Notice that the near-offset difference data point shown by a star at 10° is very close to the first scenario. Then, the far-offset data (shown by the second star at 30°) was scaled by using a constant Q-value of 80, so that the far-offset difference follows the modeled trend predicted by the rock-physics curve.

Estimating the saturation change from 1996 to 2001

In equation 13, we need the initial saturation distribution within the plume S_A. Because we do not have the 1996 offset stacks, we used a simplified method to get an estimate of this, by using the near-offset stack from 2001, and we assume that the strong anomaly observed close to the injection point is caused by the CO_2 injection. This is a reasonable assumption because we know that the pressure changes are close to zero. One remaining cause is temperature changes because we are injecting relatively cold CO_2 into a somewhat warmer reservoir (35.5°C). We will assume that the seismic impact of such temperature changes is minor.

Figure 11 shows near-offset seismic data from 2001, and we notice a clear anomaly close to the injection well. We interpret this as being caused by the CO_2 injection, and more precisely by the CO_2-saturation change. If we subtract the background average amplitude rms values, we obtain the rms map as shown in Figure 11b. We observe that the average rms level is close to 0.1 after subtracting this background amplitude value. In our case, the zero-offset reflection coefficient is approximately equal to $\Delta\alpha/2\alpha$, where α is the P-wave velocity. This means that a reflection coefficient of –0.1 corresponds to $\Delta\alpha/\alpha = -0.2$. From Figure 3, we observe that this value corresponds to a CO_2 saturation of approximately 0.1 (which means that we use $S_A = 0.1$).

An alternative way to estimate the 2001 CO_2 saturation is to use earlier publications to obtain a rough estimate. Using Arts et al. (2008), we observe from their Figure 6 that the seismic response in 2001 is distributed over approximately the same area also in depth, and that the reflectivity strength is fairly constant with depth, approximately down to the injection point (which is at 1050 m). From Kiær et al. (2015), we observe from Figure 1 in this paper that the areal extent of the uppermost layer is approximately 0.23 km^2 in 2001. Assuming a homogeneous distribution of CO_2 from the top layer to the injection point, that is over a depth range of 250 m, yields an available volume $V_a = 0.058$ km^3. We know that approximately 3 Mtons of CO_2 has been injected at Sleipner between

1996 and 2001, corresponding to a compressed volume $V_C = 0.0044$ km^3 assuming that the CO_2 density is 675 kg/m^3. Dividing these two volumes yields a very rough estimate for the average CO_2 saturation of 0.08, which is not too far from our estimate of 0.1.

Estimating the saturation change from 2001 to 2008

Using the estimated saturation change in 2001 as input to equation 13, and using the near- and far-offset differences between 2001 and 2008 as input to equation 13, we obtain the saturation in 2008 S_B. If we subtract S_A (equal to 0.1) from this, we get the saturation change between 2001 and 2008 as shown in Figure 12. Again, this estimate is meant to represent the uppermost sand layer (often referred to as layer 9, see e.g., Furre and Eiken, 2014). A smoothed version of the saturation change is also shown in this figure. We notice saturation changes to the north of the injection point and also fairly close to the injection point at the east and south side.

To combine seismic and gravity data, we need to find a way to estimate saturation changes for the entire reservoir thickness. If we use a very long window instead of the short window used so far, the algorithm should also pick up some saturation changes from deeper layers. We apply the same procedure as described above for a time window ranging from 850 to 1100 ms (which should include all layers above the injection point). A new calibration was done for this purpose, and a single scalar of 0.08 was applied to the data, and the initial saturation (Figure 13) was estimated by multiplying the near-offset amplitude change by 0.4. In this procedure, we assume that the time-lapse AVO behavior of a stack of thin layers follow the same AVO-trend as one thick layer represented by the rms amplitude over the entire layer. The accuracy of this assumption is discussed in Appendix B. The estimated saturation changes are displayed in Figure 13, showing an unsmoothed and a smoothed version. We observe that the algorithm suggests that there are practically no saturation changes in an area close to the injection point equal to approximately 1 km^2. This area corresponds more or less exactly to the estimated initial saturation change (Figure 13a). It is very likely that the 4D seismic estimates are inaccurate and underestimate the saturation changes caused by the shadow effect from the CO_2 that was occupying this volume in 2001 and the fact that saturation changes greater than 0.3 are hard to detect from seismic measurements. One way to circumvent this problem is to use the time-lapse gravity data as a complementary source of information in this area.

Time-lapse gravity

Offshore time-lapse gravity measurements have a relatively short history. This monitoring technique was possible by the development of high-precision seafloor gravimeters (Sasagawa et al., 2003). By gradual improvements of the seabed gravimeters, the repeatability between two gravity surveys was pushed from approximately 4 to 2 μGal. For the Sleipner CO_2 project, we have gravity data from 2002 and 2009 available. We used these data to constrain our saturation-inversion, and especially put weight on the gravity data in areas where we assume that the CO_2 saturation is larger than 0.3. Our gravity signal is caused by the density difference

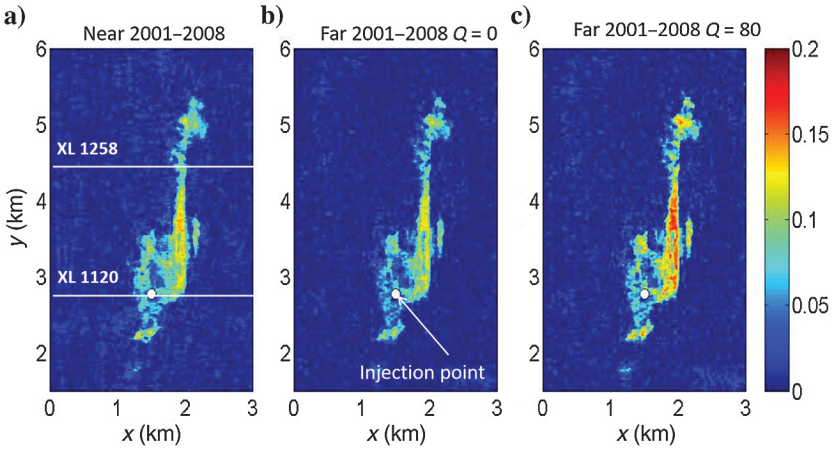

Figure 10. The rms amplitude (26 ms time window) for the (a) 2001–2008 near-offset stack difference, (b) corresponding far-offset amplitudes (no Q-compensation) and after application of (c) a constant Q-model using $Q = 80$. The white circle at approximately (1.5, 2.8) km is the CO_2-injection point. The location of the crosslines shown in Figures 6 and 7 is shown as white horizontal lines in plot (a).

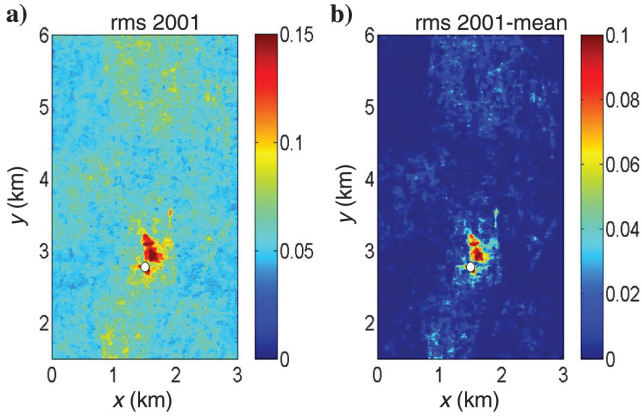

Figure 11. Near-offset reflection amplitude (rms) from (a) 2001 and (b) same data after subtracting the average value. The maximum value for this difference is 0.1, which corresponds to a relative velocity change of −0.2. The corresponding saturation change (see the dashed line in Figure 3) is approximately 0.1. This means that the plot (b) can also serve as an initial guess for the saturation changes between 1996 and 2001, without further scaling.

between supercritical CO_2 and the brine water originally trapped in the pore space within the Utsira sand layer.

Following, for instance, Keary et al. (2002; equation 6.9), we can write down the expression for the gravity anomaly caused by the CO_2 injection. We find that the gravity difference response modeled at the seabed in (x, y) is estimated by computing the following 2D integral:

$$\Delta g_{\mathrm{mod}}(x,y) = G \int dx'dy'\varphi\Delta\rho\Delta S(x',y') \times \frac{d \cdot z}{((x-x')^2+(y-y')^2+z^2)^{\frac{3}{2}}}, \quad (14)$$

where G is the gravity constant, φ is the porosity, $\Delta\rho$ is the density difference between CO_2 and water, z is the depth to the reservoir, and d is the thickness of the reservoir. Also, ΔS is the CO_2 saturation change between 2002 and 2009. Figure 14a shows the estimated gravity signal based on the smoothed saturation change estimate (Figure 13a). Because our main concern here is the spatial distribution, we have scaled the final estimated gravity change to match the maximum measured gravity change. We clearly observe from Figure 14a that there is a mismatch between the measured gravity data (shown by circles) and the modeled response based on the estimated saturation changes from 4D seismic. The white circle in Figure 14 is the injection point.

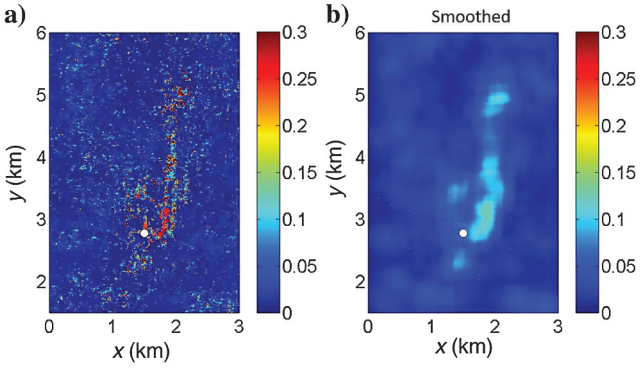

Figure 12. (a) Estimated saturation changes between 2001 and 2008 for the upper layer at Sleipner. The white circle shows the injection point. Plot (b) shows a smoothed version of the same plot.

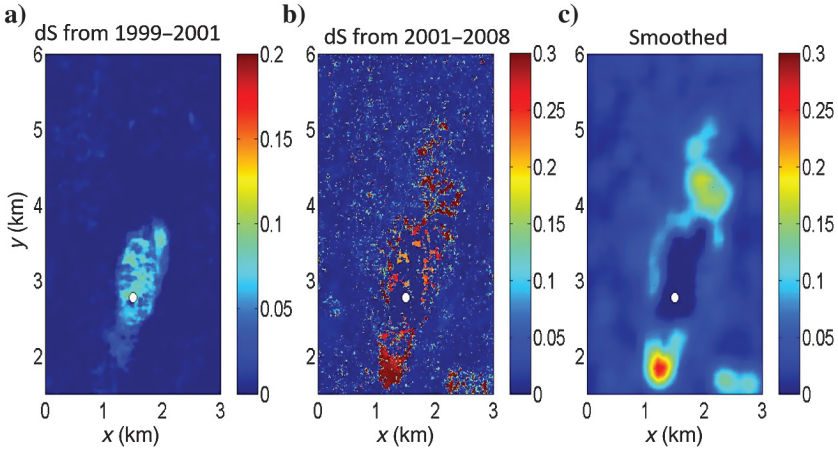

Figure 13. (a) Near-offset rms amplitude for a time window from 850 to 1100 ms, after subtracting the average value, and scaled by 0.4. This is used as an initial estimate of the average CO_2 saturation in 2001. (b) Estimated saturation changes between 2001 and 2008 from the 4D seismic data. (c) Smoothed version of the estimated saturation changes.

Now, we will use a simple inversion strategy: Let the estimated saturation changes in the areas where the estimated saturation changes are below a critical threshold S_c be scaled by a factor k to enhance the estimated saturation changes. This critical threshold is estimated by trial and error, and it is a practical number that identifies areas where the seismic shadow effect has been strong. This means that we change the modeled gravity difference given in equation 14 to be

$$\Delta g_{\mathrm{mod}}(k;x,y) = k \cdot G \int dx'dy'\varphi\Delta\rho\Delta S(x',y') \times \frac{d \cdot z}{((x-x')^2+(y-y')^2+z^2)^{\frac{3}{2}}}, \quad (15)$$

where $k = 1$ (meaning no change) if $\Delta S > S_c$. In the present example, we used $S_c = 0.03$. The risk of introducing noise in the final saturation image increases as the critical threshold decreases, so this parameter has to be determined on a trial-and-error basis. In this way, we allow the estimated saturation changes based on the time-lapse seismic data to be scaled by k for instance in the shadow zone. This means that we keep the spatial distribution of the saturation changes suggested by the time-lapse seismic inversion, but we let the measured gravity data determine how much the estimated saturation change should be *upscaled*. This means that we let the gravity data "talk" in the shadow zone, and we assume that the saturation change suggested by the time-lapse seismic inversion should be strengthened by this scalar to compensate for the seismic shadow effect and the fact that there is a low seismic sensitivity for saturation changes from 0.3 and above. To determine an optimal value for k, we use the following least-squares norm:

$$LS(\kappa) = \sum_{i=1}^{N} (\Delta g_{\mathrm{mod}}(\kappa, x_i, y_i) - \Delta g_{\mathrm{obs}}(x_i, y_i))^2, \quad (16)$$

where N is the number of gravity anomaly measurements (denoted Δg_{obs}) made at locations (x_i, y_i). By letting this factor κ vary between one and seven, we find a global least-squares error minimum between the gravity data and the modeled gravity response from the esti-

mated saturation changes at approximately 2.4, as shown in Figure 15. The optimal modeled gravity change is shown in Figure 14b, and we see that the match between the measured gravity data (shown as circles) and the modeled gravity data has improved. This is particularly true for the saddle area between the two main peaks in the modeled gravity anomaly. For other measurements, we can actually find areas where there is no improvement. However, the overall result is that the least-squares error is reduced by approximately 20%, as shown in Figure 15. The final estimated saturation changes are given as $\Delta S_{\text{final}} = k\Delta S$, where $\Delta S(x, y)$ represents the estimated saturation changes based on seismic data only. In this inversion, we used only gravity measurements that were larger than 4 μGal. The 4 μGal threshold represents the accuracy of the time-lapse gravity measurements (Alnes et al., 2011). A comparison between the initial saturation change estimate (between 2001 and 2008) and the inverted one is shown in Figure 16. We clearly see the role of the gravity data to increase the saturation changes close to the injection point.

On the lower right corners of the estimated saturation changes shown in Figure 16, there is an anomaly that we interpret as noise. If we study the rms differences for near- and far offsets (Figure 17), we notice that there is a weak difference signal in the lower right corner on the far-offset data. Because we have not implemented a cutoff related to the amplitude of the 4D differences, and we are using the difference between the near- and far-offset differences, this noise will show up as signal on the estimated saturation changes.

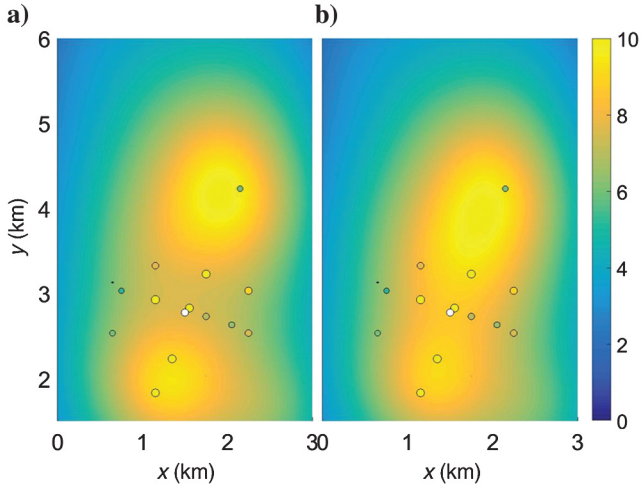

Figure 14. (a) Modeled gravity signal change based on the 4D seismic estimate of saturation change. The color bar is in microGal, and 10 μGal corresponds to a reduction of 10 μGal between 2001 and 2008. The circles show the measured gravity anomaly data. The circles are color-coded, so a huge color difference between the circle and the surrounding modeled signal means discrepancy between modeling and observations. The size of the circles is proportional to the gravity change signal. (b) Corresponding modeled gravity change, after least-squares error minimization. The injection point is shown as a white circle.

However, the uncertainties and pitfalls associated by using equation 13 for a long time window are numerous: First, there will be shadow effects and focusing/defocusing effects causing the deeper reflections to be less accurate and actually misleading to be used by a simple AVO-interface approach as proposed here. Second, remaining multiples caused by the strong reflections associated with the top layer will cause misleading results. Third, additional filling of a lower CO_2 layer will only be observed if the CO_2 saturation increases to a level that is less than 0.3. For instance, an increase in saturation from 0.3 to 0.6 will not give a large reflectivity change in the time-lapse seismic data.

Discussion

In the constrained inversion, we only used gravity data that showed a decrease in gravity, and in which the absolute value of the gravity change is larger than 4 μGal. If we include all available measurements, some of the weaker gravity signals and especially those measurements resulting in an increased gravity change will

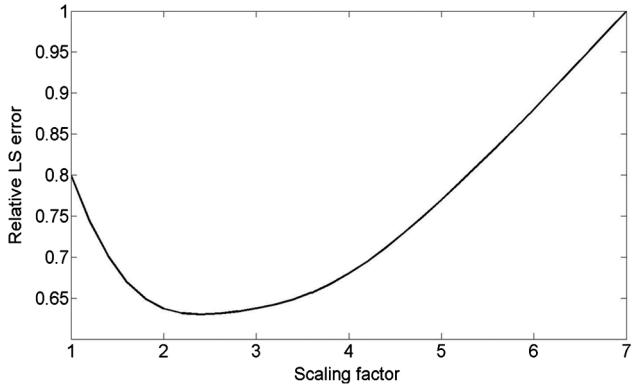

Figure 15. Relative least-squares error as a function of the scaling factor used to enhance the saturation changes in the shadow zone. The optimal scaling factor is 2.4.

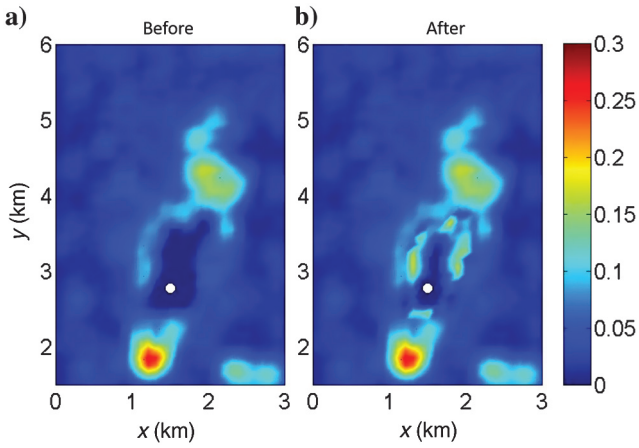

Figure 16. (a) Initial saturation change estimate between 2001 and 2008 based on the 4D seismic and inverted saturation changes constrained by a least-squares inversion using the gravity measurements.

give a very strong signal close to the injection point. In addition to this, gravity measurements that are further away from the Sleipner CO_2 site and closer to the area of gas production will be more influenced by the gas production. The Sleipner gas field is situated to the west of the Sleipner CO_2 area. We think this is misleading for the following reasons: Between the years 2002 and 2009, 5.88 Mtons of CO_2 has been injected, and, therefore, decreased gravity should be expected, especially for those measurements that are taken outside the plume. (The farther from the plume, the closer the gravity signal will be to a point source.) There are some scenarios that might create increased gravity; for instance,

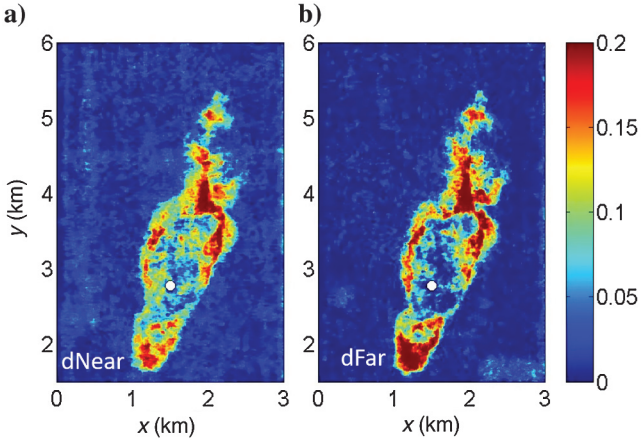

Figure 17. (a) Near- and (b) far-offset rms differences (between 2001 and 2008) using a time window from 850 to 1100 ms. Notice the weak noise in the lower right corner on the far-offset differences. These differences (although they are weak) create a noisy saturation signal (see Figure 16).

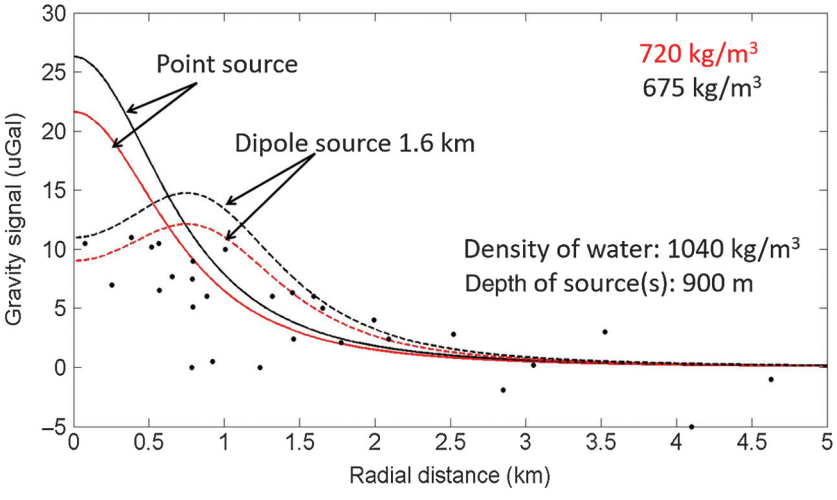

Figure 18. Change in observed gravity anomaly signals (black dots) between 2002 and 2009 plotted as a function of the radial distance from the injection point. Solid lines show point source (assuming that 5.88 Mtons of CO_2 has been injected) of gravity signals assuming that the density of CO_2 is constant and is equal to 675 (black line) and 720 kg/m^3 (red line). Density of water is assumed to be 1040 kg/m^3. A depth of 900 m has been used for the point source gravity modeling. Dashed lines show corresponding (inline) result assuming two point sources separated by 1.6 km.

if the CO_2 dissolves in water (after a time), water goes back into the plume again. In our opinion, this is not very likely to happen at a large scale. However, in a detailed mass balance computation, such an effect might influence the final result. A downward migration of the CO_2 that was in the plume in 2001 will also cause a positive gravity change, but this is also very unlikely to happen. It is much more likely that injection of 5.88 Mtons of CO_2 will cause decreased gravity, when measured right above the plume and when measured at long distances away from the plume. Therefore, we used a threshold of 4 μGal (corresponding to the uncertainty of the time-lapse gravity measurements) for the constrained inversion. Figure 18 shows a simple comparison between the measured gravity data plotted against the radial distance from the injection point. In this figure, we compare the experimental data with a simple gravity modeling assuming that 5.88 Mtons of CO_2 has been injected as a point mass at the injection point (shown by solid lines) and assuming that the same mass is distributed as two point masses separated by 1.6 km (dashed lines). The black curves represent a CO_2 density of 675 kg/m^3, whereas the red curves correspond to a density of 720 kg/m^3. We clearly see that the simple monopole distribution does not fit the data and that the two-point distribution is closer to the measurements. It should be noted that the dashed lines correspond to an inline two-point distribution. For other directions, the gravity signal will be weaker and even closer to the measurements. Compared with the best estimate of CO_2-density changes obtained by the joint inversion method (Figure 14), we observe that this estimate is far from such simple distributions: It is more like an elongated structure with a weak concentration structure in the north–south direction. This might indicate that the uppermost layers are being filled not only from several sources that are spread but also from the area close to the injection point.

How sensitive is the time-lapse AVO method to errors in the estimated calibration parameters? A simple test in which the global scaling parameter is changed from 0.06 to 0.08 is shown in Figure 19. The major effect is to increase the saturation by a constant factor. Maybe the increase is slightly less in the south compared with the north. A similar effect (but opposite in sign) is observed if the Q-factor is increased from 80 to 100: The estimated saturation changes have approximately the same spatial distribution, but the overall saturation changes are less, as shown in Figure 20. From these simple tests, we conclude that the calibration procedure does not influence the spatial distribution of the estimated saturation changes significantly, but it

changes the DC-component or the absolute value of the estimated changes.

We have chosen to use equation 13 to estimate the saturation changes, and then we use the direct relationship between saturation and density to get the density changes. This choice is related to the fact that the sensitivity for density changes on the seismic data is significantly less than that for velocity (Figure 3). However, if we use equation 9 to estimate density changes directly from the seismic data, we get a result (Figure 21) that is not too far from the saturation estimate (Figure 16a). However, it should be noted that the estimated size of the density change, 30%, is not very realistic.

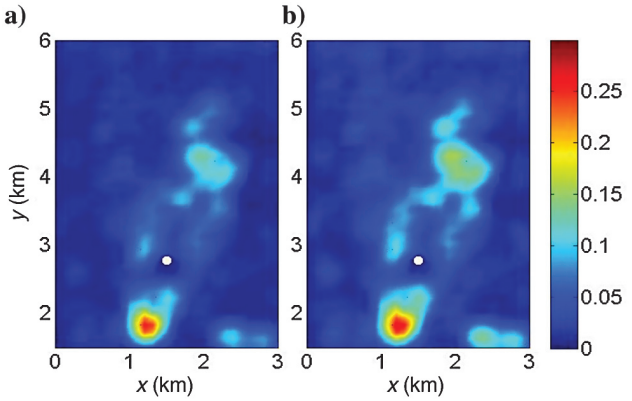

Figure 19. The effect of increasing the global scaling factor from (a) 0.06 to (b) 0.08 on the estimated saturation changes based on the time-lapse seismic data only.

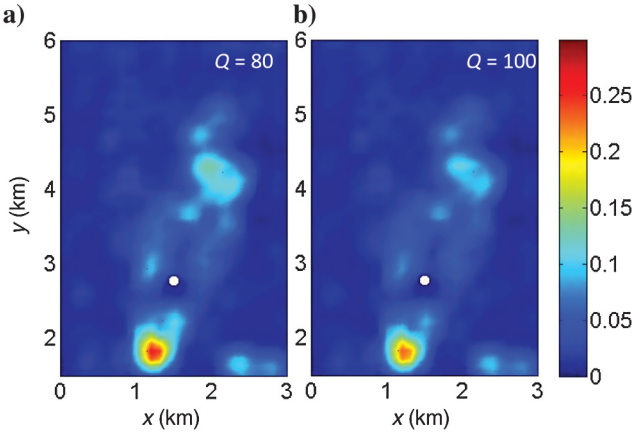

Figure 20. The effect of increasing the Q-factor from (a) 80 to (b) 100 on the estimated saturation changes based on the time-lapse seismic data (2001 and 2008) only.

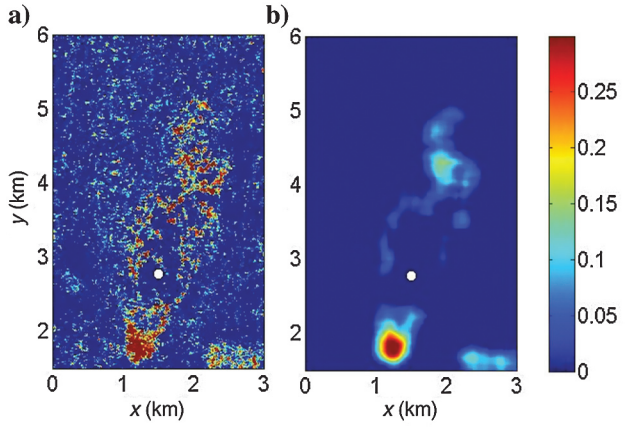

Figure 21. Estimated density changes using the time window from (a) 850 to 1100 ms using seismic data from 2001 and 2008. Plot (b) is the smoothed version.

The total amount of CO_2 injected between the 2002 and 2009 seismic surveys is 5.88 Mtons. If we use the estimated saturation change values as shown in Figure 16b, we find that the total mass of CO_2 injected in this period is equal to 7.91 Mtons. In this simple calculation, we have assumed an average reservoir thickness of 200 m and that the density difference between CO_2 and water is 230 kg/m^3. Furthermore, we have assumed that the average porosity is 0.37. The injection point is not located at the base of the Utsira sandstone unit, but at approximately 50 m above. Using 150 m for the reservoir thickness will therefore reduce the total injected CO_2 from 7.91 to 5.93 Mtons, which is much closer to the actual value. However, the uncertainties coupled to these estimates are huge, and therefore, this exercise should not be taken too seriously.

Conclusion

A calibrated time-lapse seismic method using near- and far-offset differences as input to estimate CO_2-saturation changes has been tested on field data from the Sleipner CO_2-injection site, offshore Norway. We find that this method is of limited value if the CO_2 is stored in several layers on top of each other because the time-lapse seismic data have less sensitivity to detect saturation changes in such a multilayered medium. By combining the seismic method with time-lapse gravity measurements, we demonstrate that a simple inversion procedure can be used to estimate saturation changes also in areas where multiple CO_2 layers are stacked on top of each other.

Acknowledgments

We thank Statoil and the Sleipner license partners ExxonMobil and Total for permission to use the data. A. K. Furre is acknowledged for assistance, discussions, and providing the seismic data to us. Thanks also go to Alistair Harding for helping us to load and read the data. M. Dzieciuch is acknowledged for assistance in writing MATLAB scripts. M. Landrø wants to thank Scripps for hosting him during his sabbatical stay and the Norwegian Research Council for the financial support.

Appendix A

Using a simple Q-model to calibrate near- versus far-offset stacks

From equation 13, it is evident that it is critical to determine the ratio between the near- and far-offset changes as precisely as possible. The time-lapse processing of the data has been done as accurately as possible,

but the Q-compensation has been very moderate because a relatively high Q-value of 300 has been applied to the data. Typical Q-values for overburden sediments in the North Sea is more likely to be less than 100 (Reid et al., 2001), and therefore, we introduce a simple Q-model correction term:

$$A_Q = e^{2\pi f\left(\frac{z}{\cos\theta_F}-\frac{z}{\cos\theta_N}\right)/(QV)}, \tag{A-1}$$

where Q is the quality factor, z is the depth of the Utsira Formation, f is the average frequency, and V is the average P-wave velocity for the overburden layers. The far-offset data should be divided by A_Q to correct for this absorption effect. One way to implement equation A-1 is to test various Q-values and to see how robust equation 13 is to such variations. For calibration purposes, we used a z-value of 800 m, an average frequency of 50 Hz, and an average P-wave velocity for the overburden (V) of 1800 m/s.

Appendix B

Using Backus averaging to estimate time-lapse response of a multilayered CO_2-storage site

Backus (1962) introduces a systematic way of averaging finely layered media. Using this averaging technique, Stovas et al. (2006) show that it is possible to replace a sequence of finely layered medium with one thick layer being described by average parameters and the net-to-gross ratio (N/G), which is a number describing the relative thickness of all CO_2 layers within the Utsira sand divided by the total thickness. In Stovas et al. (2006), the N/G is defined as the thickness of the sand layer divided by the total thickness of the reservoir layer. In this work, we have adapted the N/G for our purpose, and therefore, we have replaced the sand thickness by thickness of CO_2 layers. For the Sleipner case, the N/G ratio is relatively small because the thickness of each layer is of the order 5–15 m. To the lowest order, the reflection coefficient versus offset can be written as

$$R(\theta) = R_0 + G\sin^2\theta, \tag{B-1}$$

where θ is the incidence angle, R_0 is the zero-angle reflection coefficient, and G is the gradient.

If we assume that the contrasts in all elastic constants are small, equation 11 from Stovas et al. (2006) reads (note that in Stovas et al. [2006], $\Delta\rho$ and ΔV_P are dimensionless entities in contrast to this paper where $\Delta\rho/\rho$ is the corresponding dimensionless quantity):

$$\begin{aligned} R_0 &= \frac{\mathrm{N/G}}{2}\left(\frac{\Delta\alpha}{\alpha}+\frac{\Delta\rho}{\rho}\right)\\ G &= \frac{\mathrm{N/G}}{2}\left(\frac{\Delta\alpha}{\alpha}-2\frac{\beta^2}{\alpha^2}\left(\frac{\Delta\rho}{\rho}+\frac{2\Delta\beta}{\beta}\right)\right), \end{aligned} \tag{B-2}$$

where α and β denote P- and S-wave velocities, respectively. This means that to the lowest order, R_0 and G are directly proportional to the expressions for one thick layer (if we let $\mathrm{N/G} = 1$ in equation B-2, we are back to the conventional AVO formula for PP-reflections). For medium contrasts in all elastic parameters, Stovas et al. (2006) find expressions that include higher order terms in N/G. These expressions will alter the analysis done in this paper somewhat. However, if N/G is small, these terms will not change our estimates significantly. For N/G close to 0.5, these corrections will be more significant and requires using equation 17 in Stovas et al. (2006) instead of equation B-2.

References

Alnes, H., O. Eiken, S. Nooner, G. Sasagawa, T. Stenvold, and M. Zumberge, 2011, Results from Sleipner gravity monitoring: Updated density and temperature distribution of the CO_2 plume: Energy Procedia, **4**, 5504–5511, doi: 10.1016/j.egypro.2011.02.536.

Arts, R., A. Chadwick, O. Eiken, S. Thibeau, and S. Nooner, 2008, Ten years' experience of monitoring CO_2 injection in the Utsira sand at Sleipner, offshore Norway: First Break, **26**, 65–72.

Backus, G. E., 1962, Long-wave elastic anisotropy produced by horizontal layering: Journal of Geophysical Research, **67**, 4427–4440, doi: 10.1029/JZ067i011p04427.

Bai, J., and D. Yingst, 2014, Simultaneous inversion of velocity and density in time-domain full waveform inversion: 84th Annual International Meeting, SEG, Expanded Abstracts, 922–927.

Bhakta, T., and M. Landrø, 2014, Estimation of pressure-saturation changes for unconsolidated reservoir rocks with high Vp/Vs ratio: Geophysics, **79**, no. 5, M35–M54, doi: 10.1190/geo2013-0434.1.

Boait, F. C., N. J. White, M. J. Bickle, R. A. Chadwick, J. A. Neufeld, and H. E. Huppert, 2012, Spatial and temporal evolution of injected CO_2 at the Sleipner Field, North Sea: Journal of Geophysical Research, **117**, B03309.

Buland, A., M. Landrø, M. Andersen, and T. Dahl, 1996, AVO inversion of Troll Field data: Geophysics, **61**, 1589–1602, doi: 10.1190/1.1444078.

Cavanagh, A. J., and R. S. Haszeldine, 2014, The Sleipner storage site: Capillary flow modeling of a layered CO_2 plume requires fractured shale barriers within the Utsira Formation: International Journal of Greenhouse Gas Control, **21**, 101–112, doi: 10.1016/j.ijggc.2013.11.017.

Evensen, A. K., and M. Landrø, 2010, Time-lapse tomographic inversion using a Gaussian parameterization of the velocity changes: Geophysics, **75**, no. 4, U29–U38, doi: 10.1190/1.3442573.

Furre, A. K., and O. Eiken, 2014, Dual sensor streamer technology used in Sleipner CO_2 injection monitoring: Geophysical Prospecting, **62**, 1075–1088, doi: 10.1111/1365-2478.12120.

Ghaderi, A., and M. Landrø, 2009, Estimation of thickness and velocity changes of injected carbon dioxide layers from prestack time-lapse seismic data: Geophysics, **74**, no. 2, O17–O28, doi: 10.1190/1.3054659.

Grude, S., M. Landrø, and B. Osdal, 2013, Time-lapse pressure saturation discrimination for CO_2 storage at the Snøhvit field: Journal of Greenhouse Gas Control, **19**, 369–378, doi: 10.1016/j.ijggc.2013.09.014.

Helgesen, J., and M. Landrø, 1993, Estimation of elastic parameters from AVO effects in the tau-p domain: Geophysical Prospecting, **41**, 341–366, doi: 10.1111/j.1365-2478.1993.tb00574.x.

Keary, P., M. Brooks, and I. Hill, 2002, An introduction to geophysical exploration, 3rd ed.: Blackwell Publishing.

Kiær, A. F., O. Eiken, and M. Landrø, 2015, Calendar time interpolation of amplitude maps from 4D seismic data: Geophysical Prospecting, **64**, 421–430, doi: 10.1111/1365-2478.12291.

Landrø, M., 1999, Discrimination between pressure and fluid saturation changes from time lapse seismic data: 69th Annual International Meeting, SEG, Expanded Abstracts, 1651–1654.

Landrø, M., 2001, Discrimination between pressure and fluid saturation changes from time lapse seismic data: Geophysics, **66**, 836–844, doi: 10.1190/1.1444973.

Leiceaga, G. G., J. Silva, F. Artola, E. Marquez, and J. Vanzeler, 2010, Enhanced density estimation from prestack inversion of multicomponent seismic data: The Leading Edge, **29**, 1220–1226, doi: 10.1190/1.3496912.

Lindeberg, E., and P. Bergmo, 2003, The long-term fate of CO2 injected into an aquifer, *in* J. Gale, and Y. Kaya, eds., Proceedings of the 6th International Conference on Greenhouse Gas Control Technologies (GHGT-6): Pergamon, 489–494.

Queißer, M., and S. C. Singh, 2013, Localizing CO_2 at Sleipner — Seismic images versus P-wave velocities from waveform inversion: Geophysics, **78**, no. 3, B131–B146, doi: 10.1190/geo2012-0216.1.

Rabben, T. E., and B. Ursin, 2011, AVA inversion of the top Utsira Sand reflection at the Sleipner field: Geophysics, **76**, no. 3, C53–C63, doi: 10.1190/1.3567951.

Reid, F. J. L., P. H. Nguyen, C. MacBeth, R. A. Clark, and I. Magnus, 2001, Q estimates from North Sea VSPs: 71st Annual International Meeting, SEG, Expanded Abstracts, 440–443.

Roy, B., P. Anno, and M. Gurch, 2006, Wide-angle inversion for density: Tests for heavy-oil reservoir characterization: 76th Annual International Meeting, SEG, Expanded Abstracts, 1660–1664.

Roy, B., P. Anno, and M. Gurch, 2008, Imaging oil-sand reservoir heterogeneities using wide-angle prestack seismic inversion: The Leading Edge, **27**, 1192–1201, doi: 10.1190/1.2978982.

Sasagawa, G., W. Crawford, O. Eiken, S. Nooner, T. Stenvold, and M. Zumberge, 2003, A new seafloor gravimeter: Geophysics, **68**, 544–553, doi: 10.1190/1.1567223.

Span, R., and W. Wagner, 1996, A new equation of state for carbon dioxide covering the fluid region from the triple-point temperature to 1100 K at pressures up to 800 MPa: Journal of Physical and Chemical Reference Data, **25**, 1509–1596, doi: 10.1063/1.555991.

Stovas, A., M. Landrø, and P. Avseth, 2006, AVO attribute inversion for finely layered reservoirs: Geophysics, **71**, no. 3, C25–C36, doi: 10.1190/1.2197487.

Trani, M., R. Arts, O. Leeuwenburgh, and J. Brouwer, 2011, Estimation of changes in saturation and pressure from 4D seismic AVO and time-shift analysis: Geophysics, **76**, no. 2, C1–C17, doi: 10.1190/1.3549756.

Tura, A., and D. E. Lumley, 1999, Estimating pressure and saturation changes from time-lapse AVO data: 69th Annual International Meeting, SEG, Expanded Abstracts, 1655–1658.

Zumberge, M., H. Alnes, O. Eiken, G. Sasagawa, and T. Stenvold, 2008, Precision of seafloor gravity and pressure measurements for reservoir monitoring: Geophysics, **73**, no. 6, WA133–WA141, doi: 10.1190/1.2976777.

Martin Landrø received an M.S. (1983) and a Ph.D. (1986) in physics from the Norwegian University of Science and Technology. From 1986 to 1989, he worked at SERES A/S. From 1989 to 1996, he was employed at IKU Petroleum Research as a research geophysicist and manager. From 1996 to 1998, he worked as a specialist at Statoil's research center in Trondheim. Since 1998, he has been a professor at the Norwegian University of Science and Technology, Department of Petroleum Engineering and Applied Geophysics. He received the Norman Falcon award from EAGE in 2000 and the award for best paper in GEOPHYSICS in 2001. In 2004, he received the Norwegian Geophysical award, and in 2007 he received Statoil's researcher prize. He received the SINTEF award for outstanding pedagogical activity in 2009. In 2010, he received the Louis Cagniard award from EAGE, and in 2011 he received the Eni award (New Frontiers in hydrocarbons). In 2012, he received the Conrad Schlumberger award from EAGE. This includes geophysical monitoring of CO_2 storage. In 2014, he received the IOR award from the Norwegian Petroleum Directorate. He is a member of EAGE, SEG, the Norwegian Academy of Technological Sciences, and the Royal Norwegian Society of Sciences and Letters. His research interests include seismic inversion, marine seismic acquisition, and 4D and 4C seismic.

Mark A. Zumberge received a B.S. in physics from the University of Michigan and a Ph.D. in physics from the University of Colorado. He is a research geophysicist at the University of California, San Diego. He is on the faculty of Scripps Institution of Oceanography's Institute of Geophysics and Planetary Physics (IGPP). These are all applied in the marine and subaerial environments. His research interests include measurements of gravity, the development of new methods to detect crustal deformation, and investigations into new seismic sensors based on optical methods.